P-Glycoprotein (P-gp) Expressed in a Confluent Monolayer of hMDR1−MDCKII Cells Has More Than One Efflux Pathway with Cooperative Binding Sites

Poulomi Acharya,[‡,§] Thuy T. Tran,[‡,§] Joseph W. Polli,[∥] Andrew Ayrton,[⊥] Harma Ellens,[§] and Joe Bentz*[,‡]

Department of Bioscience and Biotechnology, Drexel University, Philadelphia, Pennsylvania 19104, Preclinical Drug Metabolism and Pharmacokinetics, GlaxoSmithKline, King of Prussia, Pennsylvania 19406, Preclinical Drug Metabolism and Pharmacokinetics, GlaxoSmithKline, Research Triangle Park, North Carolina 27709, Preclinical Drug Metabolism and Pharmacokinetics, GlaxoSmithKline, Welwyn, United Kingdom

Received March 26, 2006; Revised Manuscript Received September 19, 2006

ABSTRACT: The multidrug resistance transporter P-glycoprotein (P-gp) effluxes a wide range of substrates and can be affected by a wide range of inhibitors or modulators. Many studies have presented classifications for these binding interactions, within either the context of equilibrium binding or the Michaelis−Menten enzyme analysis of the ATPase activity of P-gp. Our approach is to study P-gp transport and its inhibition using a physiologically relevant confluent monolayer of hMDR1−MDCKII cells. We measure the elementary rate constants for P-gp efflux of substrates and study inhibition using pairwise combinations with a different unlabeled substrate acting as the inhibitor. Our current kinetic model for P-gp has only a single binding site, because a previous study proved that the mass-action kinetics of efflux of a single substrate were not sensitive to whether there are one or more substrate-binding and efflux sites. In this study, using this one-site model, we found that, with "high" concentrations of either a substrate or an inhibitor, the elementary rate constants fitted independently for each of the substrates alone quantitatively predicted the efflux curves, simply applying the assumption that binding at the "one site" was competitive. On the other hand, at "low" concentrations of both the substrate and inhibitor, we found no inhibition of the substrate efflux, despite the fact that both the substrate and inhibitor were being well-effluxed. This was not an effect of excess "empty" P-gp molecules, because the competitive efflux model takes site occupancy into account. Rather, it is quantitative evidence that the substrate and inhibitor are being effluxed by multiple pathways within P-gp. Remarkably, increasing the substrate concentration above the "low" concentration, caused the inhibition to become competitive; i.e., the inhibitor became effective. These data and their analysis show that the binding of these substrates must be cooperative, either positive or negative.

The human multidrug resistance transporter P-glycoprotein (P-gp)[1] (*1*) is the product of the hMDR1 gene, ABCB1, and is widely expressed in human epithelial tissue as a protection against xenobiotics. It is one of the 48 members of the ABC family of membrane transporters within the human genome (*2*). The biological and clinical significance of P-gp has been demonstrated through a large number of *in vitro*, preclinical and clinical studies (*3*−*10*). A wide variety of *in vitro* expression systems have been used to study P-gp structure and function: purified protein (*11*), lipid reconstitutions of purified P-gp (*12*−*14*), plasma membrane vesicles (*15*), suspension or unpolarized adherent cells overexpressing P-gp (*16*−*18*), and more recently, polarized confluent cell monolayers (*19*−*25*).

A key question about P-gp and any similar transporter is how many functional binding sites and efflux pathways it contains, as well as the nature of the communication between these sites. It is generally believed that the two transmembrane domains, TMDs, of P-gp form a large binding pocket (*11*, *14*, *26*, *27*). Each TMD is composed of six transmembrane α helices, and the binding pocket appears to be within the interface between α helices 4−6 in TMD 1 and α helices 9−12 in TMD 2 (*14*). If P-gp has more than one substrate-binding site and each can lead to efflux, whether through a common or a different route within P-gp, it will need to be analyzed by a multipathway kinetic model. In this case, the next question is whether the pathways are independent or cooperative.

The binding of substrates to P-gp has been assayed in many different ways, each of which is consistent, at least in some studies, with multiple substrate/inhibitor/modulator-binding sites within the P-gp-binding pocket. Lugo and Sharom (*13*) and Loo and Clarke (*14*) have recently reviewed the current hypotheses about the number of binding sites on P-gp and their possible inter-relationships. There are many different proposals on both topics.

To address these questions, we use a polarized MDCKII−hMDR1 confluent cell monolayer, which constitutively

* To whom correspondence should be addressed. Fax: 215-895-1273. E-mail: bentzj@drexel.edu.
‡ Drexel University.
§ King of Prussia.
∥ Research Triangle Park.
⊥ Welwyn.

[1] Abbreviations: P-gp, P-glycoprotein product of the hMDR1 gene; A:B>A or A:A>B, concentration in the apical chamber when the basolateral or apical chamber is the donor; B:B>A or B:A>B, concentration in the basolateral chamber when the basolateral or apical chamber is the donor.

10.1021/bi060593b CCC: $33.50 © 2006 American Chemical Society
Published on Web 11/30/2006

overexpresses P-gp in the apical plasma membrane. It has the advantage of studying P-gp in a physiologically relevant expression system, without the uncertainties of how purification and reconstitution affect function. It has the disadvantage of being a more complex expression system to analyze. We believe that all expression systems will be needed to elucidate the structure−function relationship of P-gp; however, the molecular parameters derived from P-gp transport from the confluent cell monolayer system will be essential to understand the extent to which the purified systems or other reconstituted expression systems predict the "native" function of P-gp. In particular, the sensitivity which P-gp activity appears to be showing toward lipid composition (*28*, *29*) makes the confluent cell monolayer, with an asymmetric lipid composition across the apical plasma membrane, more likely to mimic the *in vivo* environment than proteoliposomes, membrane vesicles, suspension cells, or unpolarized adherent cells.

MATERIALS AND METHODS

Materials. Amprenavir and GF120918 were from GlaxoSmithKline; loperamide was from Sigma; and quinidine was from Fisher Scientific. ^{3}H-loperamide (10 Ci/mmol) and ^{3}H-amprenavir (21 Ci/mmol) were custom-synthesized by Amersham Pharmacia Biotech, U.K. ^{3}H-quinidine (20 Ci/mmol) was from ICN Biomedical, Inc. Hoechst 33342 and rhodamine 123 was purchased from Invitrogen (Eugene, OR). Dimethyl sulfoxide (DMSO) was from Sigma-Aldrich. Dulbecco's modified Eagle's medium (DMEM) was from MediaTech, VWR. DMEM with 25 mM *N*-2-hydroxyethylpiperazine-*N*′-2-ethanesulfonic acid (HEPES) buffer, high glucose (4.5 g/L), L-glutamine, pyridoxine hydrochloride, without sodium pyruvate, and with phenol red was from Gibco. The same medium without phenol red was used for transport experiments. Transwell 12-well plates with polycarbonate inserts (0.4 μM pore size and 12 mm in diameter) were obtained from Costar (Acton, MA).

Substrate Selection. Amprenavir, quinidine, and loperamide were chosen because they are good P-gp substrates; they are chemically unrelated and show different transport and mass balance problems (*23*, *24*). Hoechst 33342 and rhodamine 123 are commonly used fluorescent substrates of P-gp (*27*).

Cell Line and Culture Conditions. The Madin−Darby Canine Kidney II cell line overexpressing human MDR1 (MDCKII−hMDR1) was purchased from The Netherlands Cancer Institute (Amsterdam, The Netherlands) (*30*). MDCK II cells were grown in 175 cm^2 culture flasks using DMEM with 10% fetal bovine serum, 1% L-glutamine, 50 units/mL penicillin, and 50 mg/mL streptomycin at 37 °C in 5% CO_2 atmosphere. Cells were split twice a week at 70−80% confluence in a ratio of 1:40, after at least 2 washes in PBS, and trypsinized with 0.25% trypsin/ethylenediaminetetraacetic acid (EDTA). All transport assays were performed with cells from passages 30 to 55. Cells were kept at 37 °C in 5% CO_2.

Single-Substrate Efflux Assay. Cells were seeded in 12-well Costar-Transwell plates with polycarbonate membrane inserts at a density of 175 000 cells per insert and grown for 4 days in culture medium. Cells were given fresh media 1 day after seeding. On the day of the experiment, culture medium was removed and cells were preincubated for 30 min with either transport medium alone or transport medium with 2 μM GF120918, a potent inhibitor of P-gp. The efflux of a range of substrate efflux across the confluent monolayer of cells was measured in both directions, that is, apical to basolateral (A>B) and basolateral to apical (B>A) in the presence and absence of GF120918. A total of 0.5 mCi/mL ^{3}H-amprenavir, ^{3}H-quinidine, or ^{3}H-loperamide was added to each respective substrate concentration to allow quantitation of efflux from donor to receiver chambers. Lucifer yellow (100 μM) was added to the donor chamber to monitor the integrity of the confluent cell monolayer. Samples (25 μL) were taken over a period of 6 h, from both donor and receiver chambers into 96-well Lumaplates and dried overnight, and the radioactivity was counted by TopCount Model 9912 (Perkin-Elmer). The initial concentration measurement was taken at 6 min after the addition of the substrate in the first well (*23*, *24*), and subsequent measurements were taken at multiple time points up to 6 h for all experiments (*24*). After a 25 μL aliquot was taken, the plates were replaced in a shaker at a speed of 30 rpm, at 37 °C in 5% CO_2. Fluorescence of lucifer yellow (excitation max = 438 nm, emission max = 530 nm) was measured at time 0 from aliquots taken directly from the vials and compared to samples taken after 6 h from both the basolateral and apical chambers into transparent bottom 96-well plates. The fluorescence was analyzed using a SpectraMax microplate reader. Passive permeability of lucifer yellow was always <10 nm/s over the entire experiment.

Inhibition Studies with Two Substrates. Cells were seeded and fed as described above, and on the day of the experiment, culture medium was removed by aspiration. The cells were then preincubated with the inhibitor/substrate in both chambers for 30 min. Note that all inhibitors used here are also P-gp substrates. During the preincubation, half of the wells receive inhibitor solution without GF120918 (to study total transport) and the other half receives inhibitor solution with GF120918 (to study passive transport). After 30 min, the preincubation solutions were removed by aspiration and the labeled substrate was added to the donor chamber, while refilling fresh inhibitor solution in both chambers, again one half without GF120918 and the other half with GF120918.

For quinidine efflux experiments using the fluorescent compounds Hoechst 33342 or rhodamine 123 as the inhibitor, the same protocol was followed. Initially, Hoechst 33342 was dissolved in distilled water, and rhodamine 123 was dissolved in absolute ethanol. Cells were preincubated for 30 min with a solution of the fluorophor in transport medium with and without GF120918 to study passive and active transport, respectively. The maximum ethanol concentration in the rhodamine transport media was <0.1%. Both basolateral and apical chambers received the same preincubation solution. After 30 min, the preincubation solution was aspirated. Donor solutions contain appropriate concentrations of quinidine, and both chambers received a fresh refill of the fluorophor, with and without GF120918. Inhibition of quinidine efflux by either of these fluorophores was studied over a period of 6 h. The radioactivity from the aliquoted samples was read using a TopCount Model 9912. Lucifer yellow was present in the donor solutions in all cases but one. For the rhodamine 123 inhibition of quinidine efflux, lucifer yellow was not used because fluorescence from rhodamine 123

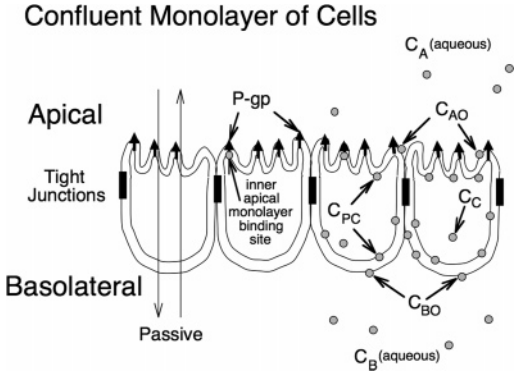

FIGURE 1: Model of a confluent cell monolayer, with the apical membrane on the top and the basolateral membrane on the bottom, where it binds to the polycarbonate insert. Passive permeability occurs in both directions. P-gp expressed on the apical membrane transports substrate from the inner apical membrane monolayer into the apical chamber. The concentration of the substrate in the apical and basolateral chambers, C_A and C_B, are measured, while the concentration of the substrate in the inner plasma membrane, C_{PC}, and the cytosol, C_C, are predicted as part of the data-fitting process described by Tran et al. (*24*).

has a significant fluorescence spectra overlap. However, the continuity of the kinetic trace of quinidine transport over 6 h showed that the monolayer remained intact.

Transport studies were performed with rhodamine 123 following the same protocol as all single-substrate transport assays. The 25 μL aliquots at specific time points were collected in transparent bottom black-sided 96-well Costar plates, and fluorescence from the aliquots was read in a Cytofluor fluorescence plate reader at an excitation wavelength of 485 nm and an emission wavelength of 530 nm with a bandwidth of 20 nm.

Cell Stability and Substrate Metabolism. We showed that the stability of the cell monolayer and plasma membrane with respect to passive and active transport was not affected by the prolonged exposure times to amprenavir for at least 6 h (data not shown; *24*). It was also shown that metabolism or decomposition was insignificant for amprenavir, quinidine, and loperamide on this time scale using radio-high-performance liquid chromatography (HPLC) (data not shown).

Numerical Integrations. We used the stiffest integrator in MATLAB, ode23s, with absolute and relative tolerances set between 10^{-8} and 10^{-10}, depending upon the data being analyzed (*24*). Other MATLAB integrators, while faster, were not accurate enough at the later times of simulations. In data fitting, all concentration curves are simultaneously fitted, so that, despite the fact that the A:B>A curve, i.e., substrate concentration in the apical chamber when the basolateral chamber is the donor, is the most visually striking, all curves contribute to minimizing the difference between the data and simulated curve. MATLAB fminsearch minimizes the coefficient of variation between the data and simulated curves. Further details can be found in refs *24* and *31*.

MASS-ACTION KINETIC MODEL

Figure 1 is a cartoon of a confluent cell monolayer, showing the polarized MDCKII−hMDR1 cells, where the basolateral membrane is attached to the polycarbonate filters and P-gp (upward arrows) is expressed on the apical surface (*32*). The apical and basolateral chambers are kept separate by the tight junctions. Active transport by P-gp occurs vectorally, with substrate binding to a site on P-gp within the apical membrane inner monolayer and with efflux into the apical chamber (*6*, *24*, *27*, *33*). For many substrates, including those we use, passive permeability is a significant fraction of total transport and is quantitatively analyzed separately using a potent P-gp inhibitor, GF120918 (*23*, *24*).

With the confluent cell monolayer system, we measure the concentration of the substrate in the apical chamber, denoted C_A, and in the basolateral chamber, denoted C_B. However, the concentration of the substrate in the cytosol, denoted C_C, and in the inner plasma membrane in contact with the P-gp-binding site, denoted C_{PC}, cannot (yet) be measured rigorously in real time. These internal concentrations are variables of a mass-action model and fitted by elementary rate constants for well-defined kinetic barriers, according to the measured values of C_B and C_A over time (*24*).

Previously, we have fitted the P-gp elementary rate constants, the passive permeability coefficients across the cell monolayer, and estimates for partition coefficients for three P-gp substrates: amprenavir [a human immunodeficiency virus (HIV) protease inhibitor], quinidine (a Na^+-channel blocker), and loperamide (an antidiarheal drug), chosen because of their very distinct behaviors as P-gp substrates (*24*). P-gp was modeled by the simplest mass-action reaction (*8*, *17*, *24*, *34*), where the binding reaction takes place within the apical membrane inner monolayer (*27*, *35*)

$$T_0 + C_{PC} \underset{k_r}{\overset{k_1}{\rightleftharpoons}} T_1 \xrightarrow{k_2} T_0 + C_A \qquad (1)$$

where T_0 is the empty transporter, C_{PC} is the substrate in the apical membrane inner monolayer, T_1 is the transporter bound by substrate, and C_A is the substrate after efflux into the apical chamber. The elementary rate constants that we seek to fit are k_1, the association rate of the substrate to P-gp from the inner apical monolayer; k_r, the dissociation rate constant of the substrate from P-gp back into the inner apical membrane; and k_2, the efflux rate constant of the substrate from P-gp into the apical chamber. We calculated the binding constant of a substrate to P-gp, relative to being in the inner apical monolayer, by the ratio of the fitted association rate constant, k_1, and the fitted dissociation rat constant, k_r, i.e., $K_C = k_1/k_r$, which is shown in Table 2 below. This means that our binding constants are for the binding sites connected to the efflux pathway. Because these binding constants are relative to the bilayer of the apical plasma membrane, they must be multiplied by the appropriate partition coefficient to get the value relative to the aqueous phase.

This reaction model has a single efflux pathway per P-gp. While it is known that P-gp can bind more than one substrate molecule, Tran et al. (*24*) showed that, with a single substrate, because the rate constant of association, k_1, was so large, the predicted efflux curves were the same whether there was one, two, or presumably, more efflux pathways in P-gp. Basically, if the binding site for one efflux pathway was filled by the substrate, then "all" sites would be filled. Thus, the number of kinetically functional efflux pathways can be probed only with the simultaneous usage of two or more different substrates.

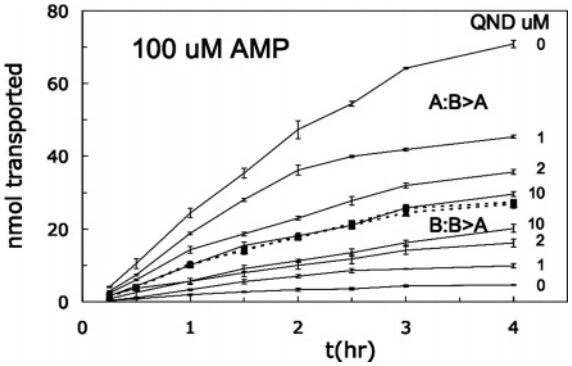

FIGURE 2: Total and passive transport of amprenavir into the receiver chamber across the monolayer of confluent MDCK cells is shown with increasing concentrations of the quinidine as the inhibitor. Transport is measured by the nanomoles of amprenavir transported over time, when the donor side begins with 100 μM amprenavir. The dotted lines show the nanomoles transported because of passive permeability (+GF120918) A:B>A, that is, to the apical chamber from the basolateral chamber marked with ■, and B:A>B, that is, to the basolateral chamber from the apical chamber marked by ▲. The two curves are nearly indistinguishable, which is expected for symmetric passive transport. Error bars are smaller than the symbols. The total transport, P-gp-mediated and passive, A:B>A is shown above the passive permeability lines as a function of the quinidine concentration (in micromolars), which is inhibiting P-gp via its own transport and, thus, reducing the amprenevir transport. The total transport B:A>B is shown below the passive permeability lines as a function of the quinidine concentration (in micromolars). Here, the inhibition of P-gp by quinidine increases the transport of amprenavir from the apical chamber. At 10 μM quinidine, the amprenavir transport is nearly the same as pure passive permeability. Error bars show triplicate standard deviations. Quinidine at the concentrations shown is preincubated with the cell monolayer for 0.5 h, and then chamber solutions are then replaced with 100 μM amprenavir in the donor chamber and fresh quinidine solution in both chambers.

The confluent cell monolayer is a challenging system to use when the aim is to obtain the elementary rate constants for P-gp activity. However, we found for this system that the standard steady-state Michaelis−Menten analysis for P-gp efflux, while commonly used and typically yielding "good fits" to data, does not provide anywhere close to accurate estimates for the Michaelis constant K_m (*31*). This was because the passive permeability across the cell membranes becomes convolved in the fitting of the K_m value, with no obvious means to deconvolve the two parameters. This suggests that classifications of P-gp transport inhibition based on the classical Michaelis−Menten steady-state kinetic formalism in other expression systems, reviewed in refs *13* and *14*, should be re-evaluated to confirm that the analysis is valid in the expression system used.

RESULTS

Amprenavir Transport Inhibited by Quinidine. Figure 2 shows the passive and total transport, which equals passive plus active, of 100 μM amprenavir, initially in the donor chamber across the MDCKII−MDR1 cell monolayers, inhibited by increasing concentrations of the P-gp substrate quinidine. The passive permeability was determined in the presence of 2 μM GF120918, a potent inhibitor of P-gp (*23*, *24*, *36*, *37*). As expected for a static passive barrier (*23*), when active efflux is inhibited with GF120918, the nanomoles of quinidine transported is symmetric (i.e., the same for B>A and A>B) over time, as shown by the closed symbols.

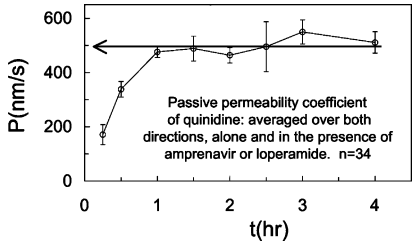

FIGURE 3: Passive permeability coefficient (+GF120918) for quinidine (QND) over 4 h in the presence of amprenavir or loperamide is shown with their respective standard deviations at each time point for all of the grouped data sets. All of the quinidine data, B>A and A>B, from 0.1−5 μM quinidine, inhibited by either 0−100 μM amprenavir (AMP) or 0−10 μM loperamide (LPM) have been included, with a total of 34 data sets. Passive permeability does not depend upon concentrations of the substrate or inhibitor. After 2 h, there is more variability, in part, because of the system approaching steady state, where the equation used to calculate the passive permeability coefficient becomes undefined (*23*). For fitting P-gp-mediated transport of quinidine, the time-dependent values of the passive permeability coefficient increase up to 1 h and then the average steady-state value calculated for 1.5 h and beyond is shown by the arrow at about 500 nm/s. For the other substrates, the crossover time from using the time-dependent passive permeability coefficients to using the steady-state average values was chosen the same way. The passive permeability coefficient of loperamide in the A>B direction increased to roughly 550 nm/s at 2 h and then declined steadily to roughly 400 nm/s; therefore, all of the time-dependent passive permeability coefficients were used.

Without GF120918, P-gp increases total amprenavir transport in the B>A direction and decreases total transport in the A>B direction. Quinidine, a P-gp substrate, was used as the inhibitor over the concentration range of 1−10 μM. Quinidine is preincubated with the cells, in both chambers, for 30 min before the chambers are emptied by aspiration, and fresh quinidine is added to both chambers along with radiolabeled amprenavir added to the donor chamber. Thus, during the amprenavir transport, the quinidine concentration is maintained close to the concentration initially added, despite its own transport by P-gp. Clearly, the active transport of amprenavir is inhibited by increasing quinidine concentrations.

Passive Permeability Is Time-Dependent and Not Affected by Inhibitors. Tran et al. (*23*) derived an exact equation for calculating the passive permeability coefficient at multiple time points, even when there is a loss of substrate into the cells, e.g., because of the binding to intracellular components. Figure 3 shows the passive permeability coefficient for quinidine over time in the presence of many amprenavir or loperamide concentrations, as well as with GF120918. We have aggregated all passive permeability coefficients for the 0.1−5 μM quinidine data in both directions, B>A and A>B, either alone or with inhibitors: amprenavir (50 and 100 μM) or loperamide (0−10 μM). There are 34 different data sets represented in this figure.

Clearly, the passive permeability coefficient of quinidine increases for the first hour of transport and is basically constant thereafter, where the arrow shows the steady-state passive permeability coefficient across the confluent cell monolayer to be about 500 nm/s in both transport directions.

Table 1: IC_{50} Ranges for P-gp Substrates

substrate (concentration range)	inhibitor (concentration range)	IC_{50}	comments
amprenavir (50 and 100 μM)	quinidine (0−20 μM, $n = 9$)[a]	2−5 μM	B>A was inhibited slightly more than A>B
quinidine (0.1−3 μM, $n = 4$)	amprenavir (0, 50, and 100 μM)	~100 μM	only two AMP concentrations tested because the solubility limit reached above 100 μM
quinidine (0.1−5 μM, $n = 5$)	loperamide (0−10 μM, $n = 8$)	5−8 μM	
quinidine (1−5 μM, $n = 4$)	Hoechst 33342 (0−10 μM, $n = 5$)	2−5 μM	Hoechst 33342 inhibits at the same concentration range as quinidine
loperamide (1−5 μM, $n = 4$)	quinidine (0−30 μM, $n = 10$)	B>A, 5 μM A>B, ≥5−20 μM	fraction inhibition stalled at about 0.5

[a] n = number of different concentrations tested from the sequence of 0, 0.1, 0.3, 1, 2, 3, 5, 10, 20, and 30 μM.

There is no significant dependence upon the inhibitor concentration or the direction of transport. The same basic results were found for the amprenavir passive permeability coefficient in the presence of quinidine, which increased for the first 0.5 h before reaching the steady state (data not shown; *24*).

For amprenavir and quinidine, this early time-dependent increase in the passive permeability coefficient is not due to substrate "loading" into the cells, because there is no significant loss of these substrates into the cells (data not shown; *23*, *24*). The change occurs on the time scale of plasma membrane recycling and may be due to changes in cell membrane area or cell microvilli morphology, as discussed below and by Tran et al. (*23*). This is true because the passive permeability coefficient that we calculate is per unit area of insert of the Transwell apparatus, i.e., 1.13 cm^2. For the fitting of P-gp transport, this is not a problem, because the passive permeability is fitted independently, to accurately calculate the active transport because of P-gp.

The passive permeability coefficient of loperamide shows an asymmetric time-dependent change, with a greater increase for A>B than B>A, which appears to be coupled with its absorption within the cells (data not shown; *23*). However, the presence of quinidine did not affect the time dependence of the change of the passive permeability coefficient of loperamide. We conclude that the presence of these inhibitors, at the concentrations used, does not significantly affect the (time-dependent) passive permeability coefficients of substrates through the confluent cell monolayer, which certainly implies that they do not affect the bilayer structure significantly.

Inhibition as Measured by IC_{50}. We began the analysis of substrate inhibition of P-gp in a semiquantitative way. Inhibition is typically represented by a curve showing the reduction of P-gp-specific transport at a particular time versus the inhibitor concentration. In the B>A direction, P-gp transport is defined as the total nanomoles transported, solid lines in Figure 2, minus the passive transport (+GF120918), dotted lines in Figure 2. This P-gp-specific transport is normalized by dividing each value by the value in the absence of the inhibitor, yielding the fraction of P-gp transport. Thus, in the B>A direction, the fraction of P-gp transport is 1 without inhibitor and decreases as the inhibitor concentration increases. The inhibitor concentration at which the fraction of P-gp transport is 0.5 is defined as the IC_{50}. In the A>B direction, this calculation would give negative numbers, because P-gp inhibits total transport; therefore, we used the absolute value to show the fraction of P-gp transport.

We have collected our measured IC_{50} values in Table 1, measured after 2 h of transport, which looks basically the same as the curves calculated at 4 h of transport. It is important to note here that these times are chosen to focus on steady-state P-gp transport. For the substrates that we use with the confluent cell monolayer, it requires 1−3 h for binding to P-gp to reach the steady state (*24*, *31*). Using shorter times for "initial rates" predominantly measures just the passive permeability coefficients. This semiquantitative analysis has been performed for each of the P-gp substrates that we use, and they all can inhibit each other. For the transport of loperamide, inhibition by quinidine in the B>A direction has an IC_{50} in the range of 5−8 μM quinidine but, in the A>B direction, inhibition seems to stall at around a fraction of 0.5 for 10−30 μM quinidine, suggesting a more complex interaction for loperamide with P-gp and the cells. Our IC_{50} values agree with those published by Rautio et al. (*25*).

Ling and co-workers have made the case that Hoechst 33342 and rhodamine 123 bind to different sites in P-gp and that rhodamine 123 binding can enhance the efflux of Hoechst 33342 (*15*, *35*, *38*). Their studies used plasma membrane vesicles purified from P-gp-expressing CH*B30 cells. The membrane vesicles were assayed to be about 50% inside out; therefore, the fluorophores would not have to pass through a bilayer to reach the P-gp-binding site of these vesicles, i.e., within the cell's inner monolayer of its plasma membrane. We found that Hoechst 33342 inhibited quinidine with an IC_{50} that was about the same as the IC_{50} of quinidine for amprenavir and loperamide.

On the other hand, we found no inhibition of quinidine transport with up to 100 μM rhodamine 123. Tang et al. (*39*) claimed that there were fluorescence quenching artifacts between Hoechst 33342 and rhodamine 123, which obscured the interpretations of the studies by Ling and co-workers. We measured the transport of rhodamine 123 across the confluent cell monolayer and found that its passive permeability coefficient is about 20 nm/s B>A and 10 nm/s A>B, i.e., more than an order of magnitude smaller than quinidine (Figure 2) and close to values reported by Tang et al. (*39*). This implies that it would take over 24 h for 50% transport to occur (*23*). This time course cannot be followed with this cell line, because is it enough time for these cells to start overgrowing themselves and obscuring the analysis. Interestingly, because the intracellular volume of the entire confluent cell monolayer is so small, crudely estimated at 1 μL (*24*), the intracellular concentration would be predicted to be essentially the same as the donor side

concentration after 2 h, using the equations by Tran et al. (*23*), although this would be difficult to prove.

We also found that the transport of rhodamine 123 was enhanced over passive permeability in the B>A direction, which would be expected if it were a P-gp substrate. However, there was no inhibition of transport in the A>B direction, as would be expected if it were not a P-gp substrate. The ambiguity of these findings will require additional work, beyond the scope of this study.

These IC_{50} analyses show that each of the P-gp substrates that we use can inhibit the other, but that proves nothing about the inhibition mechanism. Because we have shown for the confluent monolayer system that the classical Michaelis−Menten analysis cannot predict K_m values to better than 1−3 orders of magnitude (*31*), there is no reason to assume that the canonical textbook Lineweaver−Burke or Eadie−Hofstee curves for competitive, uncompetitive, and/or mixed competition are applicable to the confluent cell monolayer system. Instead, we will pursue the question of the mechanism with a rigorous analysis of the mass-action transport by P-gp.

Inhibition as Measured by Mass-Action Kinetic Analysis of a One-Site Model for P-gp. Our current P-gp transport model only has a single binding site for P-gp (*24*, *31*). However, writing a two-binding site model and fitting the data does not prove that the model is correct, because more parameters will be available to fit the data. More importantly, writing such a model and implementing it requires a clear idea of the most important molecular parameters. With this in mind, here, we are asking the simpler but essential question of what kind of mechanisms can be tested by a one-site model. This is a prerequisite to writing a minimal two-site model, i.e., the one that captures the important mechanisms with the fewest number of parameters. Because we use only P-gp substrates, neither uncompetitive nor mixed-type competition are relevant, as defined by the classical Michaelis−Menten analysis. Basically, there are two classical Michaelis−Menten mechanisms and one other mechanism that can be tested against the data. (1) Competitive inhibition: Inhibitor replaces the substrate in "the single" P-gp-binding site. This is the simplest case expected for combinations of substrates. When transport data fits this model, it does not prove that P-gp has only one binding site. (2) Noncompetitive inhibition: All P-gp bound initially to the inhibitor is thereafter "inactivated", because the inhibitor concentration is constant throughout our experiments. This classical mechanism is simple to test, but it is rare with soluble enzymes. The transport data present here is nowhere near the predictions from this mechanism, and we will not consider it further. (3) No-inhibitor effect: Despite substantial transport of the inhibitor, there is no effect on substrate transport. Setting the inhibitor concentration to 0 in the simulation of substrate transport tests this mechanism, i.e., ignoring its presence and its known P-gp-mediated efflux. This is direct kinetic evidence of the substrate and inhibitor being effluxed by independent pathways within P-gp, under the specific conditions used. This caveat is very important, because it foreshadows our finding that the "mechanism" will shift according to pathway occupancy. This mechanism has also been called noncompetitive in the transport literature. We believe the nomenclature used here is less likely to be confused with mechanism 2, mentioned above.

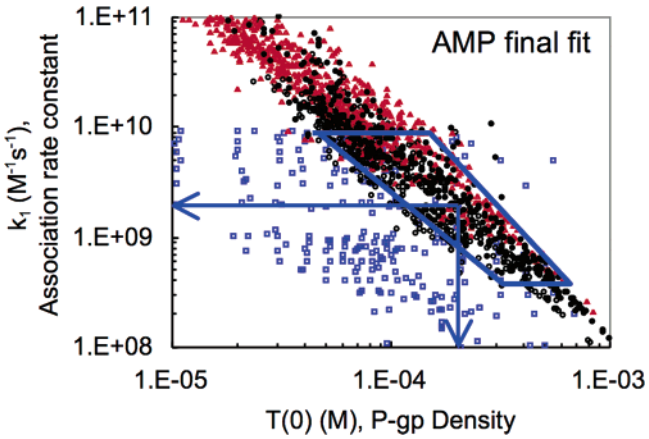

FIGURE 4: Distribution of the best fitting pairs of the density of efflux-active P-gp, $T(0)$, and the association rate constant, k_1, for amprenavir alone is shown, following the fitting algorithm explained in ref *24*. The amprenavir concentrations are color-coded (black, 10 μM; red, 30 μM; and blue, 100 μM). The pairs of $\{T(0), k_1\}$ randomly distributed within the box, which looks like a tilted trapezoid shown in blue, give essentially identical best fits to the data for all of these substrate concentrations. The arrows point to parameter values at the "center of the box". Table 2 shows these values, i.e., $k_1 = 2 \times 10^9$ M^{-1} s^{-1} and $T(0) = 200$ μM in the inner apical monolayer, which equals 160 P-gp/μm^2 in the apical membrane (see footnote *b* in Table 2).

For this study, we have refitted all of the elementary kinetic parameters for single-substrate studies of amprenavir (AMP), quinidine (QND), and loperamide (LPM) using new data. Because Tran et al. (*24*) described the kinetic analysis in detail, we will only discuss the outcomes. The fitting algorithm developed by Tran et al. (*24*) finds all of the possible values of the parameters $\{T(0), k_1, k_r, k_2\}$ that can best fit the data for each of the substrate concentrations used. $T(0)$ denotes the initial density of efflux-active P-gp, Not surprisingly, there are many different combinations that give essentially the same best fits to the data, but they are clustered into a compact set, i.e., a seemingly random collection of equally good fitting parameters within a closed area, which is a benchmark for the validity of this kinetic analysis.

Figure 4 shows the final fitting for the best fit $\{T(0), k_1\}$ pairs found in this study for amprenavir transport, without any inhibitor. The different-colored symbols denote different amprenavir concentrations, from many separate experiments. The subset of $\{T(0), k_1\}$ pairs within the blue box, which looks like a tilted trapezoid, fit all of the substrate data equally well and are called the consensus fits (*24*). The pairs outside of the box only fit the data for some substrate concentrations. Values of the association rate constant $k_1 > 1 \times 10^{10}$ M^{-1} s^{-1} are excluded because that is at or above an upper bound for substrate lateral diffusion through the bilayer (*24*). P-gp densities above 8000 P-gp/μm^2 or 0.01 M in the apical membrane (see footnote *b* in Table 2) are excluded because that would require the plasma membrane to be entirely covered by close packed P-gp (*24*). P-gp densities below 1 P-gp/μm^2, i.e., 4 orders of magnitude lower than the maximum, are excluded as being too small. Otherwise, the fitting algorithm has no constraints.

The blue arrows in the "center of the box" show the values for each parameter, which are the values shown in Table 2, only to 1 significant digit. All of the fitted parameters come from the "center of the box" of parameter values for the substrates tested, with a range of about a factor of 3 for $T(0)$

Table 2: Fitted Parameter Values with Single-Substrate Experiments

substrate	"V_{max}" $k_2T(0)$[a] (M/s)	efflux-active P-gp density T(0)[b] (μM)	association to P-gp k_1[c] ($M^{-1}\,s^{-1}$)	efflux to apical chamber k_2[d] (s^{-1})	dissociation to apical membrane k_r[e] (s^{-1})	partition coefficient K_{PC}[f]	binding bonstant K_C (M^{-1})[g] cytosolic dissociation constant "$K_{D,Aq}$" (M)	steady-state passive permeability coefficients[h] (nm/s)
AMP	3×10^{-2}	200	2×10^9	150	2×10^6	200	1000	$P_{BA} = 420 \pm 50$
							"5 μM"	$P_{AB} = 400 \pm 50$
QND	1×10^{-3}	200	2×10^9	5	1×10^5	700	15 000	$P_{BA} = 500 \pm 100$
							"0.1 μM"	$P_{AB} = 500 \pm 100$
LPM	4×10^{-4}	200	2×10^9	2	5×10^5	3000	4000	$P_{BA} = 350 \pm 80$
							"0.1 μM"	$P_{AB} = 400 \pm 100$

[a] The product of $k_2T(0)$ is very rigorously fitted by the first step in the algorithm, and the values shown were fixed by at least the first 100 best fits, which all has the same coefficient of variation, CV; i.e., these are robust fits at each concentration. For loperamide, the fits were taken from the higher concentrations only, $\geq 5\ \mu$M. Lower concentrations did not yield as many stable fits, although the integrated curves using these parameters look reasonable. As mentioned in the Results, loperamide fits require a basolateral transporter, which is inhibited by GF120918, i.e., the P-gp inhibitor. [b] The "center of the box" efflux-active concentration of P-gp within the inner apical monolayer, as shown in Figure 4 for amprenavir. These units can be converted to a more typical form, assuming a 2 nm lipid monolayer thickness for the acyl chain region. $T(0)$ (P-gp/μm^2) = $0.8T(0)$ (μM, inner apical monolayer) = 160 P-gp/μm^2. The ratio of the apical membrane to the insert cross-section area is irrelevant, because it cancels out in the calculation. [c] Center of the box estimate for the association rate constant k_1. As shown for amprenavir in Figure 4, the range was $k_1 = (1-10) \times 10^9\ M^{-1}\,s^{-1}$. For quinidine and loperamide, the range was broader, $k_1 = (0.2-10) \times 10^9\ M^{-1}\,s^{-1}$ (data not shown; *24*). [d] Center of the box estimate for the efflux rate constant k_2, from P-gp into the apical chamber, given by the ratio of the fitted $k_{21}T(0)$ for each substrate and the center of the box value of $T(0) = 2 \times 10^{-4}$ M. See the text and footnote *b* above. [e] Center of the box estimate for the dissociation rate constant k_r, from P-gp back into the inner apical monolayer. [f] Equilibrium substrate partition coefficient to 0.1 μm PS/PE/chol (1:1:1) liposomes. This lipid composition is a rough mimic for the inner apical monolayer, as described in ref *24*. [g] The binding constant to P-gp from the inner apical monolayer, defined by $K_C = k_1/k_r$. Below each binding constant, we show in parentheses the appropriate dissociation constant for each substrate relative to the aqueous cytosol, calculated as $K_{D,Aq} = 1/(K_C \times$ drug partition coefficient{PS/PE/chol}). These dissociation constants are more than an order of magnitude smaller than the IC_{50} values shown in Table 1 and the K_m values derived from a steady-state Michaelis−Menten analysis of these data (*31*). [h] Steady-state passive permeability coefficients measured across the confluent cell monolayer, in the presence of the P-gp inhibitor GF120918, as shown in Figure 3 for quinidine after 1 h. P_{BA} is shown first, and P_{AB} is shown underneath. The values are not always symmetric, because the passive permeability for loperamide is faster in the A>B direction than in the B>A direction before their convergence at steady state. This was also observed in ref *23*.

and the rate constants (see below). More precise estimates are limited by experimental error and computational expense. These values are quite adequate for our purposes here and are best fits for the data.

From Table 2, we see that the efflux-active density of P-gp, $T(0)$, is independent of the substrate, which was a crucial test of the model and the fitting algorithm, because it should not depend upon the identity of the substrate (*24*). The association rate constant, k_1, is also independent of the substrate, which agrees with the open structure of P-gp for substrates with similar molecular weights (*24*, *40*).

On the other hand, the efflux rate constants, k_2, the passive permeability coefficients in both directions across the confluent cell monolayer, P_{BA} and P_{AB}, the binding constants to P-gp from the inner apical monolayer, K_C, and the partition coefficients, K_{PC}, are all substrate-specific, as expected.

In the column showing the binding constants of the substrates to P-gp, there is also shown an effective aqueous dissociation constant for each substrate, $K_{D,Aq}$, which is calculated as the inverse of the product of the binding constant times the partition coefficient to the liposomes, composed of 1:1:1 phosphatidylethanolamine (PE)/phosphatidylserine (PS)/cholesterol (chol) as the mimic of the inner apical monolayer. It estimates the aqueous concentration expected to give 50% binding to P-gp, in the absence of the inhibitor. This number is not near the steady-state K_m that would be fitted using a standard Michaelis−Menten steady-state analysis (*31*), because that analysis does not work for the confluent cell monolayer. These effective dissociation constants are 20−100 times smaller than the IC_{50} values shown in Table 1, showing that the IC_{50} cannot predict the dissociation constant of the substrate when it is used as an inhibitor. For the confluent cell monolayer, an IC_{50} is purely phenomenological and dependent upon many factors besides the substrate-binding constant, e.g., the substrate passive permeability. This result will be elucidated in a separate study.

There are two significant differences between some of these values and those published by Tran et al. (*24*). The first difference is minor, in that the binding constants for loperamide and quinidine to P-gp found here are just above the upper bounds found by Tran et al. (*24*). The values quoted here fit all of the data better.

The other difference is physiologically quite interesting. In Figure 4, the shape of the consensus box for the {$T(0)$, k_1} pairs is somewhat different than that found by Tran et al. (*24*), which yields roughly a 2−3 fold larger estimate for the center of the box value for the density of efflux-active P-gp, $T(0)$, while the estimate for k_1 is essentially the same. In addition, the passive permeability coefficients for all three substrates are roughly 2−3 fold larger than reported by Tran et al. (*24*). The similar increase in two biophysically "unrelated" parameters suggests a common mechanism. These differences do not affect our analysis of the inhibition mechanism, but they are very important for the *in vivo* activity of P-gp, which will be discussed below. This kinetic modeling is providing a high-resolution view of the transport data and can uncover differences that would be very difficult to notice or prove otherwise.

For the inhibition experiments, the inhibitor is preincubated with the cells in both chambers for 30 min before the substrate is added to the donor chamber, with a refreshment of the inhibitor concentration in both chambers at that time to ensure that the transport of the inhibitor does not change its concentration dramatically during the transport experiment. A crucial part of the fitting process is using the passive permeability coefficients at all time points to correct the total

transport for the contribution of passive permeability. As explained by Tran et al. (*24*), this correction must be done within the mass-action equations for transport, rather than simply subtracting the nanomoles transported passively from the total nanomoles transported, which neglects transport reversibility. All of these passive permeability coefficients increase in time until a steady state is reached, as shown in Figure 3 for quinidine. For fitting active transport, we use the individual values for each time point, e.g., up to 1 h for quinidine, until the steady state is reached. Thereafter, the average value within the steady-state period is used, as shown in Figure 3 for quinidine by the arrow at about 500 nm/s. This approach avoids fitting the noise of the passive permeability coefficient (*24*).

Competitive Inhibition versus No-Inhibitor Effect. We can now move to the mechanism of inhibition of P-gp efflux by P-gp substrates. These data will be shown as the substrate concentration over time in both chambers, because this is the form of the data actually being fitted. The different concentrations are labeled in the figures by a short notation. For example, A:B>A is read as the concentration of substrate in the apical chamber when the basolateral chamber is the donor and the apical chamber is the receiver.

Figure 5 shows a sample of the data and fits for the P-gp-mediated transport of quinidine when amprenavir is the inhibitor. Figure 5A shows 0.3 μM quinidine transport in the presence of 100 μM of the inhibitor amprenavir. Data are shown by the symbols with error bars defined by the standard deviation of triplicate measurements. All simulations used the single-substrate parameters shown in Table 2; i.e., there is no fitting of these data with the inhibitor. The solid lines show the case where binding to the "single P-gp site" is competitive, using the binding constants shown in Table 2. The dashed lines show the case where there is no inhibitor effect; i.e., the concentration of amprenavir is set to 0 in the simulation of the dashed line in the figure. This is equivalent to amprenavir following a different efflux pathway within P-gp than the one used by quinidine. Clearly, competitive inhibition fits the data much better than the no-inhibitor effect curve. Note that the color of the data, blue for basolateral and red for apical, must match the color of the simulation curves for the data to fit. Likewise, the data symbols must match, with □ for B>A flux, where the basolateral chamber is the donor, and △ for A>B flux, where the apical chamber is the donor.

Competitive inhibition is the simplest expectation for two substrates. This does not prove that P-gp has only one efflux pathway. Doubling the number of "competitive" pathways in P-gp would have little effect on the total transport because one of the most important fitted parameters is the product of the efflux rate constant and the density of efflux-active P-gp, $k_2T(0)$, which is the equivalent of V_{max} in the language of the Michaelis−Menten analysis (*24*). This parameter is very tightly fixed (*24*), so that, if we simply proposed that P-gp had twice the number of pathways, the efflux rate constant k_2 would become half as large as that shown in Table 2. This makes sense, because the overall substrate efflux would be the same in both cases and that is what is being fitted.

Figure 5B shows the data and fits for the P-gp-mediated transport of 0.3 μM quinidine, now in the presence of only 50 μM of the inhibitor amprenavir, i.e., half of the concentration as in Figure 5A. If quinidine and amprenavir still competitively bind to the "single P-gp site", then the solid curves should fit the data just as well as the case above. The fact that less amprenavir and more quinidine would be bound is taken into account by the equations for competitive inhibition. Remarkably, the data is fitted better by the case of the no-inhibitor effect. It is important to pay attention here to the donor side curves, B:B>A and A:A>B, where the no-inhibitor effect simulations predict a slower loss of quinidine from the apical donor side than for the basolateral donor side, which is what the data shows. The competitive inhibition simulations predict the same rate of quinidine loss from both donors, which was what was observed in Figure 5A with the larger amprenavir concentration but not with 50 μM amprenavir.

Before continuing, it is important to explain that we decided to use this plot format because it can prove the mechanism most compactly. The conventional plot of nanomoles transported per micromolars of inhibitor will show inhibition only at adequately high concentrations, regardless of whether inhibition is always competitive or there is no inhibitor effect at the low concentrations. If binding is competitive, then inhibition will only occur when enough inhibitor had bound to replace some bound substrate. However, if the mechanism transitions from the no-inhibitor effect to competitive once the "amounts bound" exceed some limits, which is the case here, then the conventional curve will show the no-inhibitor effect until the mechanism shifts over to competitive inhibition. The qualitative inhibition curve will look the same, except that the "binding constant" of the inhibitor will appear weaker than it actually is. To prove that the no-inhibitor effect occurs, it must be shown that the amount of inhibitor needed to cause competitive inhibition is greater than that predicted by the independent binding constants. The plot format that we use shows this comparison simply and directly.

We will see below that there is substantial amprenavir transport by P-gp under similar conditions; thus, this P-gp-mediated transport of amprenavir must be through a different pathway than that used by quinidine here. All of the combinations of concentrations shown in Table 1 have been analyzed. The data presented in the figures were picked to show roughly the minimal concentrations needed to provide competitive inhibition and the maximal concentrations allowed to show no inhibitor effect. The message is simple. When the substrate and inhibitor concentrations are both small enough, there is no inhibitor effect, despite the fact that there is P-gp-mediated transport of the inhibitor transport. For example, in Figure 6A, 50 μM amprenavir shows substantial transport in the presence of 2 μM quinidine, i.e., 7 times more quinidine than in Figure 5B.

The next result is even more interesting. Figure 5C shows the data and fits for the P-gp-mediated transport of 3 μM quinidine, i.e., a 10-fold increase of the substrate concentration with the same 50 μM amprenavir as the inhibitor. Here, the best fit is back to competitive inhibition. Therefore, when amprenavir is relatively saturating P-gp, 100 versus 50 μM, or quinidine is relatively saturating P-gp, 3 versus 0.3 μM, then the inhibition is competitive. An increase in the substrate concentration, 0.3−3 μM quinidine, causes the inhibitor, 50 μM amprenavir, to transition from the no-inhibitor effect to competitive inhibition. This novel result proves that the

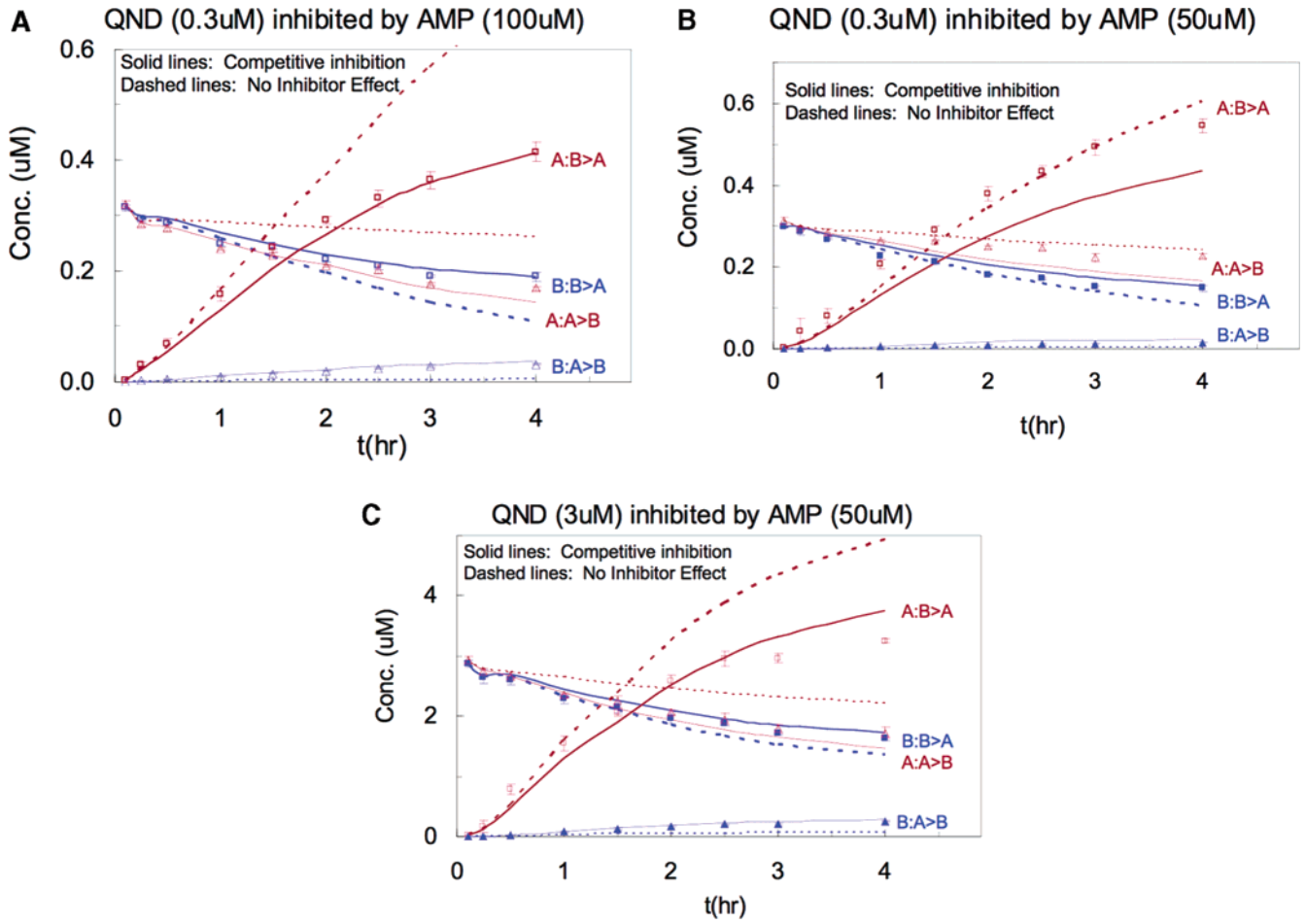

FIGURE 5: Data and fits for the P-gp-mediated transport of quinidine with amprenavir as the inhibitor. All four transport curves are shown here and in the same way in Figures 5−7. For all figures, red denotes concentrations from the apical chamber and blue denotes concentrations from the basolateral chamber. All data symbols are open, because P-gp is active in all cases shown, with □ for B>A data and △ for A>B data, as used above. Simulations use the parameters given in Table 2, with either the assumption that the substrate and inhibitor are competing for the "single" P-gp-binding site (—) or the assumption that there is no inhibitor effect (- - -). Because it is very important to identify which simulation best fits the data, we have made the simulations have thick lines for the B>A direction and thin lines for the A>B direction. From top to bottom, the curves are denoted A:B>A (open red squares), for the concentration of the substrate in the apical chamber when the basolateral chamber is the donor; B:B>A (open blue squares), for the concentration of the substrate in the basolateral chamber, blue, when the basolateral chamber is the donor; A:A>B (open red triangles), for the concentration of the substrate in the apical chamber when the apical chamber is the donor; and B:A>B (open blue triangles), for the concentration of the substrate in the basolateral chamber when the apical chamber is the donor. Data are shown by the symbols with error bars defined by the standard deviation of triplicate measurements. A shows 0.3 μM quinidine transport in the presence of 100 μM amprenavir as the inhibitor. Competitive inhibition fits the data very well, while the no-inhibitor effect does not. B shows 0.3 μM quinidine transport in the presence of 50 μM amprenavir as the inhibitor. The no-inhibitor effect fits the data very well, as if there is no amprenavir in the system, while competitive inhibition does not. There is substantial transport of amprenavir under these conditions (see Figure 6 below). C shows 3 μM quinidine transport in the presence of 50 μM amprenavir as the inhibitor. Competitive inhibition fits the data very well, while the no-inhibitor effect does not. As explained in the text, many other cases were tested, and the cases shown in the figures were chosen to show the substrate and inhibitor concentrations marking the transition between the no-inhibitor effect and competitive inhibition.

binding sites for efflux pathways are cooperative, as shown in the Supporting Information. Therefore, we are seeing a mixing of mechanisms driven by binding site occupancy.

Here, we want to show other substrate combinations to determine the generality of this observation. Figure 6 shows the data and fits for the P-gp-mediated transport of amprenavir when quinidine is the inhibitor. Figure 6A shows the data and fits for the P-gp-mediated transport of 50 μM amprenavir in the presence of 2 μM quinidine. The best fit is for the no-inhibitor effect. Therefore, even 2 μM quinidine is not enough to yield competitive inhibition. However, as shown in Figure 6B, the P-gp-mediated transport of 50 μM amprenavir in the presence of 5 μM of the inhibitor quinidine is mostly competitive. Therefore, the transition from the no-inhibitor effect to competitive inhibition is gradual rather than abrupt, at least on a population average.

We now turn to loperamide, which appears to have a more complex interaction with these cells than quinidine and amprenavir (*23*, *24*). Figure 7 shows the data and fits for the P-gp-mediated transport of quinidine when loperamide is the inhibitor. Figure 7A shows the data and fits for the P-gp-mediated transport of 1 μM quinidine in the presence of 2 μM loperamide. The best fit is for the no-inhibitor effect. Figure 7B shows the data and fits for the P-gp-mediated transport of 3 μM quinidine in the presence of 10 μM of the inhibitor loperamide. The best fit is competitive. We also studied the P-gp-mediated transport of 50 and 100 μM amprenavir when loperamide is the inhibitor. There was no inhibitor effect with 50 μM amprenavir inhibited by 1 μM

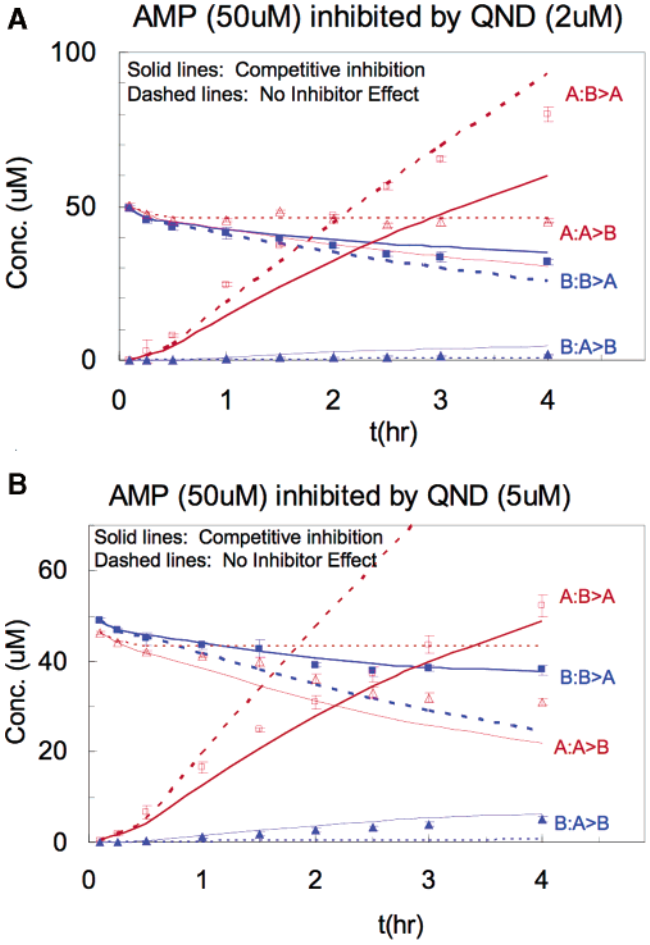

FIGURE 6: Data and simulations for the P-gp-mediated transport of amprenavir with quinidine as the inhibitor, using the same nomenclature as in Figure 5. A shows 50 μM amprenavir transport in the presence of 2 μM quinidine as the inhibitor. The no-inhibitor effect fits the data very well, as if there is no quinidine in the system, while competitive inhibition does not. There is substantial transport of quinidine under these conditions (see Figure 5 above). B shows 50 μM amprenavir transport in the presence of 5 μM quinidine as the inhibitor. Competitive inhibition fits the data very well, while the no-inhibitor effect does not.

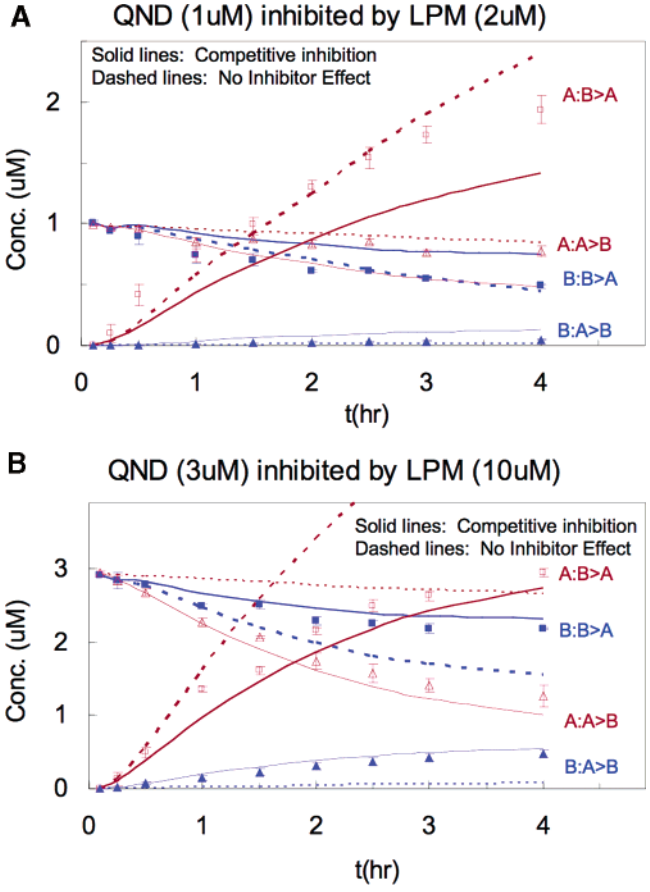

FIGURE 7: Data and simulations for the P-gp-mediated transport of quinidine with loperamide as the inhibitor, using the same nomenclature as in Figure 5. A shows 1 μM quinidine transport in the presence of 2 μM loperamide as the inhibitor. The no-inhibitor effect fits the data very well. B shows 3 μM quinidine transport in the presence of 10 μM loperamide as the inhibitor. Competitive inhibition fits the data very well, while the no-inhibitor effect does not.

loperamide and competitive inhibition with 2−10 μM loperamide. The transport of 100 μM amprenavir was competitively inhibited by 1−10 μM loperamide (data not shown).

Loperamide is inhibited by quinidine; however, the inhibition was incomplete in the A>B direction (Table 1). Complete inhibition of P-gp-mediated transport of loperamide can only be achieved with very high quinidine concentrations, >20 μM, where there is little P-gp-mediated transport (data not shown). This suggests that loperamide has an additional interaction with these cells and/or P-gp beyond those that are well-modeled for amprenavir and quinidine, as noted previously by Tran et al. (*24*). Our current hypothesis is that there is another transporter in the basolateral membrane, which admits loperamide and is completely inhibited by GF120918. Because the cell line used is canine kidney epithelial, there are many candidates (*41*). We can say that quinidine and amprenavir have no significant interaction with this putative transporter, at any concentration used (data not shown). When loperamide is an inhibitor, the putative transporter only makes more certain that the preincubation achieves steady state in loperamide. We will present the inhibition of loperamide transport by these other P-gp substrates in a separate paper, because this is outside the scope of this work. The bottom line is that the existence of this putative loperamide transporter does not affect our conclusion that P-gp has multiple pathways, at least for amprenavir and quinidine.

DISCUSSION

It is known that P-gp can bind more than one substrate at a time (*13*, *14*). However, Tran et al. (*24*) showed that the efflux kinetics of a substrate, without any inhibitor, was predicted to be the same whether each P-gp had one or two efflux binding sites. Because the association rate constant to P-gp was so large, effectively lipid lateral diffusion-controlled, if one site was occupied, then all sites were occupied. Equilibrium binding and/or ATPase activity could not have predicted this. To understand the activity of P-gp efflux with the confluent cell monolayer, the mass-action kinetics of efflux must be studied directly and rigorously, i.e., not with the steady-state Michaelis−Menten equations (*31*). To determine the number of efflux pathways of P-gp, it is necessary to use more than one substrate at a time.

Inhibition of P-gp by its substrates and modulators has been intensely studied, as reviewed by Lugo and Sharom (*13*) and Loo and Clarke (*14*). From many assays, including

transport, it has been found that some pairs of substrates do not compete with one another, at the particular concentrations studied, which has been called a noncompetitive interaction. We define this mechanism as the no-inhibitor effect, to not confuse it with the classical noncompetitive inhibition mechanism for enzymes. This observation lent support to the work of Ling and co-workers, who have made the case that Hoechst 33342 and rhodamine 123 are P-gp substrates that bind to different sites in P-gp and that rhodamine 123 binding can enhance the efflux of Hoechst 33342, suggesting distinct pathways through P-gp (*15*, *35*, *38*; see also refs *27* and *39*). Additional quasi-independent pathways have been proposed (*42*). Of course, there may be other binding sites for modulators of P-gp activity that do not lead to efflux of that modulator.

For single substrates, we show binding constants to P-gp from the inner apical monolayer in Table 2. In fact, these binding constants were calculated from the ratio of the fitted values of the association rate constant k_1 and the dissociation rate constant k_r, from P-gp back into the inner apical monolayer, i.e., $K_C = k_1/k_r$ (M^{-1}). This means that the binding constants that we measured are for the binding sites of the efflux pathways.

Our analysis yields a fairly simple picture of substrate binding and efflux for P-gp, at least for quinidine and amprenavir, as well as inhibition by loperamide, a trio of drugs chosen solely because of their different behaviors as P-gp substrates (*23*, *24*). Using the elementary rate constants fitted for these substrates alone, we found that, at "high" concentrations of substrate and/or inhibitor, the substrate efflux curve was fitted very well with the sole assumption that the substrate and inhibitor competed for the "single" P-gp-binding site. The fit does not imply that each P-gp has only one binding site but only that all sites behave as though they are independent at the substrate and inhibitor concentrations used.

At low concentrations of the substrate and inhibitor, the efflux of the substrate was unaffected by the presence (and efflux) of the inhibitor. Under these conditions, we found that the efflux of the substrate was still quantitatively predicted using the elementary rate constants fitted for each of the substrates alone, with the sole assumption that the inhibitor did not bind to the "single site" of the substrate; i.e., it must use another site and efflux pathway. This proves that P-gp has two or more efflux pathways. The gradual transition from the no-inhibitor effect to competitive inhibition as the concentration of either the substrate or inhibitor increases suggests that both the substrate and inhibitor can bind to all of the efflux connected binding sites, as their individual binding constants prescribe. It has been proposed that these binding sites are flexible or, to some extent, inducible (*43*). We will need to build the two-site efflux model to fit and simulate the gradual transition from the no-inhibitor effect to competitive inhibition to better understand the mechanistic implications of this finding.

It is very important to mention that the ability of the one site model to fit the competitive inhibition data is a strong validation of our kinetic model and fitting algorithm. The analysis presented by Tran et al. (*24*) is rather complex within the field of P-gp transport kinetics. That was a consequence of our belief that a clear understanding of P-gp efflux activity *in vivo* could only come from applying the most rigorous kinetic analysis to the most physiologically relevant expression system. The fact that the density of efflux-active P-gp in the cell membrane was found to be independent of the substrate type was required if the model and the fitting algorithm were valid. The lipid lateral diffusion-controlled value of the association rate constant, k_1, was also independent of substrate type, which agrees with the predicted openness of the structure of P-gp within the plasma membrane (*24*, *40*).

However, because the fitted value of k_2 is different for each substrate, it could be argued that the parameter that we fit is not really the efflux rate constant from P-gp but rather represents a distinct and unknown barrier for each substrate. We just fit a parameter in an equation, which does not prove that the parameter is the claimed rate constant for P-gp efflux. There are good reasons why our assignment of k_2 to the efflux rate constant of P-gp is reasonable (*24*), but that does not eliminate the question. Because we are fitting three rate constants and a P-gp membrane density simultaneously, such an argument must be constantly checked against the data.

The fact that the single-substrate parameters for amprenavir and quinidine can quantitatively fit the competitive inhibition data would be hard to explain if the fitted k_2 was not the P-gp efflux rate constant for each substrate. It is nearly certain now that the fitted k_2 must come from the same barrier for all three substrates. The fitting process is so blind and so exhaustive, leaving no potential fit undiscovered, that we are now far more confident that the k_2 that we fit is the efflux rate constant for P-gp.

Spoelstra et al. (*16*) found evidence of the inhibitor concentration affecting the "mechanism" of P-gp efflux. They studied the interaction of daunorubicin with verapamil, both P-gp substrates, in multidrug-resistant cell lines grown as a monolayer on plates and fitted their data with a Michaelis−Menten steady-state model for the no-inhibitor effect, using our terminology. However, at a higher daunorubicin concentration, there was a shift away from this model. They proposed two daunorubicin binding sites in P-gp, with verapamil binding to the weaker site, so that the high concentration of daunorubicin would be required to competitively inhibit verapamil transport.

What do our kinetic findings about transport tell us about the interaction between the efflux binding sites, i.e., cooperativity? The key observation was that an increased substrate concentration causes the inhibitor to increase its competitive inhibition of substrate transport. Without the inhibitor, increased substrate concentrations do not "inhibit" transport in any way, as shown here and by Tran et al. (*24*). A single binding constant and a single efflux rate constant fit all of the substrate concentration curves. Of course, this must not be confused with the fact that P-gp-mediated transport does become saturated with an increased substrate concentration, thus making the fraction of total transport because of P-gp smaller relative to passive permeation. The transition from the no-inhibitor effect to competitive inhibition means that the efflux of the substrate is less than it would have been without the inhibitor.

Basically, the increased substrate concentration must increase the efficacy of the inhibitor either through the binding constants, $K_C = k_1/k_r$, or the efflux rate constants, k_2. Obviously, an increase in the substrate concentration must cause an increase in the amount of substrate bound. If the

efflux rate constants, k_2, are responsible for the transition toward competitive inhibition, then the bound substrate must inhibit the flow of other substrate molecules or enhance the flow of inhibitor molecules through the other efflux pathways, relative to having the inhibitor bound to those other efflux binding sites. How this could happen, when the substrate alone does not show the same effect, is very unclear. Any proposed mechanism along these lines will require a complex feedback loop, and there is no data or theory supporting such a concept at this time.

It is easy to believe that cooperative binding between the two or more efflux binding sites could cause the transition from the no-inhibitor effect to competitive inhibition with an increased substrate concentration. To prove this, we have carried out a rigorous and general analysis of the two-site binding model in the Appendix (which is posted in the Supporting Information). Interestingly, many different combinations of positive and/or negative cooperativity can predict the increased inhibitory effect with an increased substrate concentration. This is an important finding for the binding model to be robust, because all of the different pairs of P-gp substrates may have very different interactions within the binding pocket (see also ref *14*).

While there has been much speculation about P-gp efflux cooperativity based on equilibrium binding and/or ATPase activity, this is the first prediction about binding based on efflux kinetics alone, insofar as we are aware. In fact, because our binding constants are obtained from efflux kinetics, they are for the efflux binding sites of the active P-gp in the plasma membrane. While the binding model analyzed here is "only" two-site, which entails a fair amount of complexity, the rigorous analysis of a three- or four-site binding model would likely reach the same conclusion. It is interesting that recently published theoretical structures for P-gp only proposed two or three binding sites, while the binding pocket appeared to be fairly "crowded" with transmembrane helices (*44*, *45*), providing ample possibilities for cooperativity.

This study provides important guidance for our construction of the two-site transport model for P-gp, because we now know that cooperativity must be part of that model. The cooperativity terms in the model will not just be extra parameters for fitting the data but rather will be required to fit the transition between the no-inhibitor effect and competitive inhibition observed for the substrates used here.

Now, we can discuss our finding that two of the fitted parameters changed from values published in ref *24*. We now find that the density of efflux-active P-gp, $T(0)$, is about 2−3 times larger and that the steady-state passive permeability coefficient for all three substrates is about 2−3 times larger than the respective values reported by Tran et al. (*24*), as shown in Table 2. We note that k_1 and k_2 did not change significantly, strongly suggesting that the change is not in P-gp, per se. Cells in culture do change or respond to subtle changes in the composition of the plastic supports (*32*), and the result that we observe is really an example of the analytical power of our kinetic analysis. We know which parameters changed and by how much, which would not be possible using, for example, the Michaelis−Menten steady-state equations (*31*).

Although the confluent cell monolayers were cultured the same way in all studies, to the extent possible, there was a hiatus of about a year between the end of data acquisition for Tran et al. (*24*) and the beginning of the studies reported here. The parameter values in Table 2 have been found consistently; e.g., Figure 3 incorporates 17 separate experiments completed over the course of more than a year. The fact that the P-gp efflux-active density changed, that the passive permeability coefficients changed, and that both changes are about the same magnitude suggests that the simplest explanation will be one that affects both "equally". An increase in the expression level of P-gp is unlikely to change passive permeability coefficients and vice versa.

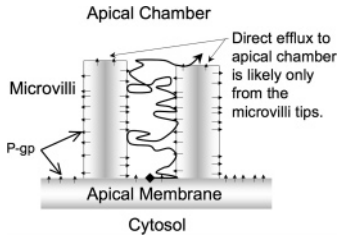

FIGURE 8: Representation of microvilli on the apical surface of MDCK II cells with P-gp expressed on the membrane by arrows. A cartoon path is shown of a random walk of a substrate molecule after being released either by P-gp or by passive permeability at the base of a microvillus. The path will involve many subsequent interactions with the same or a neighboring microvillus. Only substrates released at the tip of the microvilli will have a reasonable chance of diffusing nonstop into the apical chamber and being counted as a result of transport mediated by efflux-active P-gp or via passive permeability. Any change in the microvilli dimension would affect the probability of escape nonstop and, hence, the number of efflux-active P-gp and the membrane area for passive permeability.

The simplest explanation that ties the density of efflux-active P-gp with the passive permeability coefficient is the random walk that the substrate must make between the microvilli subsequent to leaving the outer apical monolayer, either by efflux by P-gp or by permeation through the bilayer or tight junction. Figure 8 shows a roughly scale model cartoon of a pair of microvilli, which are about 10 μm high, 1 μm in diameter, and separated by 1 μm.

By definition in the kinetic model, the P-gp that are efflux-active are those that send their substrate directly into the apical chamber, where it equilibrates "instantly" between the sampling volume of the apical chamber and the outer apical monolayer, according to the partition coefficients. Tran et al. (*24*) found that the surface density of efflux-active P-gp was probably 10−20 times smaller than the total P-gp estimated in Ambudkar et al. (*47*) for a related cell line. While the cell lines were not identical and expression levels for our line have not been quantitiated, we felt that the difference was significant and hypothesized that only P-gp at the tips of the microvilli will be efflux-active for our fitting. This does not mean that the rest of the P-gp do not efflux, but rather, the random walk of the substrate released from P-gp into the aqueous space at the base of a microvillus will almost certainly encounter the same or a neighboring microvillus rather than escaping nonstop into the apical chamber. Absorption back into the outer apical monolayer and flip-flop into the inner apical monolayer would put the substrate back to where it started, and the cycle would have to be restarted. Only those substrate molecules that are released from P-gp at or near the tips of the microvilli would have a reasonable probability of escaping directly into the apical chamber. Our current data increases the efflux-active

P-gp to about 3−10 times smaller than that estimated in ref *47* for the related cell line.

The 2−3 times larger steady-state passive permeability coefficient for all three substrates reported here, relative to values reported in ref *24*, can be explained by the same hypothesis. Recall that the passive permeability coefficients are calculated relative to the surface area of the plastic inserts that the cells are grown on, i.e., 1.14 cm^2, because we cannot know the true membrane surface area (*23*, *24*). A change in the cell monolayer surface area that can directly release the substrate into the apical chamber will change the passive permeability coefficient that we report. Obviously, microvilli morphology can change this true membrane surface area, and the changes that we see occur on the time scale of membrane recycling, e.g., Figure 3 (*48*).

Thus, in Figure 8, the diffusion pathway shown will also apply to a substrate released at the base of the microvilli by passive diffusion through the bilayer or tight junction. Changes in the morphology of the microvilli would have to change both the number of efflux-active P-gp and the passive permeability. It is difficult to conjure another mechanism that explains both changes so parsimoniously. If this hypothesis is correct, then the morphology of the microvilli is an important component of the *in vivo* activity of P-gp, as well as for this cell line.

We have performed a simple test calculation for this hypothesis using a very simple model for the aqueous space between adjacent microvilli. We have simulated a random walk away from a square well sunk into an infinite plane, 1 μm on all four sides and 10 μm deep. The question is whether a particle released from the side of the well, like the side of the microvilli, will escape to the apical chamber or be reabsorbed into the wall or plane. The test particle was released 1 nm from the wall or plane, and its 3D random walk was followed until it hit another wall of the square well, the infinite plane, or escaped into the apical chamber by reaching 10 μm from the top of the plane. To get reliable statistics, we examined 10^8 test particle releases. Relative to the escape frequency from the plane 1 μm away from the edge of the well, like the tip of the microvillus, the probability of escape starting from the top edge of the well, midway between the corners of the well, was just 0.38. Particles that had entered into the well had a much smaller chance of eventually escaping than particles that never entered the well. This probability of escape was reduced nearly exponentially as the test particle was released further down the side of the well, mimicking being released from the sides of the microvilli, to 0.013 when the release was 1 μm into the well and to 0.000 83 when the release was 2 μm into the well. Escape from the bottom of the well, like the release point shown in Figure 8, was at least 8 orders of magnitude less probable, i.e., not 1 of 10^8 released particles escaped. It is a highly simplified model of escaping from the microvilli without being reabsorbed, but it shows that the basic hypothesis is physically sound.

CONCLUSIONS

We have three general conclusions about P-gp efflux kinetics. The first is that the specific mechanism of binding and inhibition does not change the efflux kinetics of P-gp by a large amount, about 2-fold at most, as shown in Figures 5−7. The no-inhibitor mechanism predicts greater efflux by P-gp than the competitive inhibition mechanism, as it must. On the basis of our findings and the literature, it seems that the general model for P-gp substrates moves from the no-inhibitor effect to competitive inhibition as P-gp becomes saturated with either the substrate or inhibitor. However, this difference appears to not produce much selective pressure on P-gp to extend the concentration range wherein the no-inhibitor effect operated and, thus, where the kinetics of substrate efflux would be somewhat larger.

The second general observation concerns the long-standing speculation about whether P-gp effluxes the substrate into the apical aqueous space or delivers the substrate in the outer apical monolayer as a flippase, followed by passive diffusion into the aqueous space (*14*, *49*). Our kinetic model for P-gp has efflux into the apical aqueous space with an instantaneous equilibration between the apical chamber and the outer apical monolayer, on the basis of the estimated partition coefficients, eq 1 and ref *24*. If we had chosen to follow the flippase model, then what was delivered to the outer apical membrane would be instantaneously equilibrated with the apical aqueous chamber. The assumption of instant equilibration was based on data showing that similar types of molecules bind to liposomes very rapidly, within seconds, compared with the kinetics of efflux over hours from the confluent cell monolayer (*24*). Explicitly including the kinetics of substrate permeation from the outer apical monolayer to the aqueous space of the apical chamber or vice versa would have doubled the number of mass-action differential equations needed to fit the data, to fit these on- and off-rate constants to the bilayer. That would have been computationally too expensive.

Loo and Clarke (*14*) are quite right that determining which of these two mechanisms P-gp follows will require very rapid stopped-flow kinetic techniques. However, if P-gp efflux is into the aqueous space, because of the initial ATP binding or its hydrolysis, then the mechanism of release is likely passive diffusion of the substrate out of the binding pocket subsequent to a decrease in its binding constant to P-gp. That means that, after leaving the extracellular domain of P-gp, the "effluxed" substrate will be within a nanometer or so of the bilayer. The random walk back to the bilayer would be common and not take long, according to our simple random walk simulation described just above. As seen from the perspective of kinetics, there is very little difference between the two mechanisms. Our kinetic model fits the efflux data assuming a maximal recycling of the substrate, where it is free to rebind to the outer apical monolayer as soon as it leaves P-gp. This shows, regardless of whether it is a flippase or a transporter, that P-gp protects the cell in part by keeping the xenobiotics occupied at the plasma membrane, as well as by facilitating their diffusion away from the apical bilayer of the cell.

Our fitted rate constants support this view of how P-gp does its job. Comparing the efflux rate constant, k_2, with the dissociation rate constant, k_r, shows that the bound substrate is 10^4-10^5 times more likely to be released back into the inner apical membrane than being effluxed into the apical aqueous compartment. Because the association rate constant, k_1, is so large, rapid dissociation back into the membrane is required for P-gp to maintain relatively weak binding for a very broad class of substrates. This means that

the selective pressure on P-gp, with respect to keeping xenobiotics out of the cytosol, is to keep k_2 larger than the passive permeation rate of the substrate through the inner apical monolayer into the cytosol. We do not know this permeability coefficient but, using the overall permeability coefficients shown in Table 2, we estimate that the rate constant for release into the cytosol is at least an order of magnitude smaller than the efflux rate constants, k_2, shown in that table.

The third general observation concerns the similarity of the efflux mechanism between P-gp and the related multidrug-resistance-related transporters, MRPs. Borst et al. (*50*) review the current transport data of MRPs and favor a model in which the binding pocket can bind more than one ligand, allowing for cooperative interactions between ligands, rather than the alternative model of requisite cotransport of two different ligands. The similarity with the P-gp mechanism is clear.

SUPPORTING INFORMATION AVAILABLE

Transition in the mechanism from the no-inhibitor effect to competitive inhibition with an increased substrate concentration that proves that the P-gp-binding sites must be cooperative (Appendix). This material is available free of charge via the Internet at http://pubs.acs.org.

REFERENCES

1. Juliano, R. L., and Ling, V. (1976) A surface glycoprotein modulating drug permeability in Chinese hamster ovary cell mutants, *Biochim. Biophys. Acta. 455*, 152−162.
2. Dean, M., Rzhetsky, A., and Allikmets, R. (2001) The human ATP-binding cassette (ABC) transporter superfamily, *Genome Res. 11*, 1156−1166.
3. Lown, K. S., Mayo, R. R., Leichtman, A. B., Hsiao, H. L., Turgeon, D. K., Schmiedlin-Ren, P., Brown, M. B., Guo, W., Rossi, S. J., Benet, L. Z., and Watkins, P. B. (1997) Role of intestinal P-glycoprotein (MDR1) in interpatient variation in the oral bioavailability of cyclosporine, *Clin. Pharmacol. Ther. 62*, 248−260.
4. Schinkel, A. H. (1998) Pharmacological insights from P-glycoprotein knockout mice, *Int. J. Clin. Pharmacol. Ther. 36*, 9−13.
5. Goh, L. B., Spears, K. J., Yao, D., Ayrton, A., Morgan, P., Roland, W. C., and Friedberg, T. (2002) Endogenous drug transporters in *in vitro* and *in vivo* models for the prediction of drug disposition in man, *Biochem. Pharmacol. 64*, 1569−1578.
6. Borst, P., and Elferink, R. O. (2002) Mammalian ABC transporters in health and disease, *Ann. Rev. Biochem. 71*, 537−592.
7. Gottesman, M. M. (2002) Mechanisms of cancer drug resistance, *Annu. Rev. Med. 53*, 615−627.
8. Ambudkar, S. V., Kimchi-Sarfaty, C., Sauna, Z. E., and Gottesman, M. M. (2003) P-glycoprotein: From genomics to mechanism, *Oncogene 22*, 7468−7485.
9. Englund, G., Hallberg, P., Artursson, P., Michaelsson, K., and Melhus, H. (2004) Association between the number of coadministered P-glycoprotein inhibitors and serum digoxin levels in patients on therapeutic drug monitoring, *BMC Med. 2*, 1−8.
10. Balayssac, D., Authier, N., Cayre, A., and Coudore, F. (2005) Does inhibition of P-glycoprotein lead to drug−drug interactions? *Toxicol. Lett. 156*, 319−329.
11. Higgins, C. F., and Linton, K. (2004) The ATP switch model for ATP transporters, *Nat. Struct. Mol. Biol. 11*, 918−926.
12. Sharom, F. J., and Eckford, P. D. (2003) Reconstitution of membrane transporters, *Methods Mol. Biol. 227*, 129−154.
13. Lugo, M. R., and Sharom, F. J. (2005b) Interaction of LDS-751 and rhodamine 123 with P-glycoprotein: Evidence for simultaneous binding of both drugs, *Biochemistry 44*, 14020−14029.
14. Loo, T. W., and Clarke, D. M. (2005) Recent progress in understanding the mechanism of P-glycoprotein-mediated drug efflux, *J. Membr. Biol. 206*, 173−185.
15. Shapiro, A. B., and Ling, V. (1997) Positively cooperative sites for drug transport by P-glycoprotein with distinct drug specificities, *Eur. J. Biochem. 250*, 130−137.
16. Spoelstra, E. C., Westerhoff, H. V., Pinedo, H. M., Dekker, H., and Lankelma, J. (1994) The multidrug-resistance-reverser verapamil interferes with cellular P-glycoprotein-mediated pumping of daunorubicin as a non-competing substrate, *Eur. J. Biochem. 221*, 363−373.
17. Stein, W. D. (1997) Kinetics of the multidrug transporter (P-glycoprotein) and its reversal, *Physiol. Rev. 77*, 545−590.
18. Seelig, A., and Gatlik-Landwojtowicz, E. (2005) Biophysical characterization of inhibitors of multidrug efflux transporters: Their membrane and protein interactions, *Med. Chem. 5*, 135−151.
19. Tang, F., Horie, K., and Borchardt, R. T. (2002) Are MDCK cells transfected with the human MRP2 gene a good model of the human intestinal mucosa? *Pharm. Res. 19*, 765−772.
20. Tang, F., Horie, K., and Borchardt, R. T. (2002) Are MDCK cells transfected with the human MDR1 gene a good model of the human intestinal mucosa? *Pharm. Res. 19*, 773−779.
21. Troutman, M. D., and Thakker, D. R. (2003) Novel experimental parameters to quantify the modulation of absorptive and secretory transport of substrates by P-glycoprotein in cell culture models of intestinal epithelium, *Pharm. Res. 220*, 1210−1224.
22. Troutman, M. D., and Thakker, D. R. (2003) Efflux ratio cannot assess P-glycoprotein-mediated attenuation of absorptive transport: Asymmetric effect of P-glycoprotein on absorptive and secretory transport across caco-2 cell monolayers, *Pharm. Res. 20*, 1200−1209.
23. Tran, T. T., Mittal, A., Gales, T., Maleeff, B., Aldinger, T., Polli, J. W., Ayrton, A., Ellens, H., and Bentz, J. (2004) An exact kinetic analysis of passive transport across a polarized confluent MDCK cell monolayer modeled as a single barrier, *J. Pharm. Sci. 93*, 2108−2123.
24. Tran, T. T., Mittal, A., Aldinger, T., Polli, J. W., Ayrton, A., Ellens, H., and Bentz, J. (2005) The elementary mass action rate constants of P-gp transport for a confluent monolayer of MDCKII−hMDR1 cells, *Biophys. J. 88*, 715−738.
25. Rautio, J., Humphreys, J. E., Webster, L. O., Balakrishnan, A., Keogh, J. P., Kunta, J. R., Serabjit-Singh, C. J., and Polli, J. W. (2006) In vitro P-glycoprotein inhibition assays for assessment of clinical drug interaction potential of new drug candidates: A recommendation for probe substrates, *Drug Metab. Dispos.*, in press.
26. Gottesman, M. M., and Pastan, I. (1993) Biochemistry of multidrug resistance mediated by the multidrug transporter, *Annu. Rev. Biochem. 62*, 385−427.
27. Lugo, M. R., and Sharom, F. J. (2005a) Interaction of LDS-751 with P-glycoprotein and mapping of the location of the R drug binding site, *Biochemistry 44*, 643−655.
28. Modok, S., Heyward, C., and Callaghan, R. (2004) P-glycoprotein retains function when reconstituted into a sphingolipid and cholesterol rich environment, *J. Lipid Res. 45*, 1910−1918.
29. Troost, J., Lindenmaier, H., Haefeli, W. E., and Weiss, J. (2004) Modulation of cellular cholesterol alters P-glycoprotein activity in multidrug-resistant cells, *Mol. Pharm. 66*, 1332−1339.
30. Evers, R., Kool, M., Smith, A. J., van Deemter, L., de Haas, M., and Borst, P. (2000) Inhibitory effect of the reversal agents V-104, GF120918 and Pluronic L61 on MDR1 P-gp-, MRP1- and MRP2-mediated transport, *Br. J. Cancer 83*, 366−374.
31. Bentz, J., Tran, T. T., Polli, J. W., Ayrton, A., and Ellens, H. (2005) The steady-state Michaelis−Menten analysis of P-glycoprotein mediated transport through a confluent cell monolayer cannot predict the correct Michaelis constant K_m, *Pharm. Res. 22*, 1667−1677.
32. Butor, C., and Davoust, J. (1992) Apical to basolateral surface area ratio and polarity of MDCK cells grown on different supports, *Exp. Cell Res. 203*, 115−127.
33. al-Shawi, M. K., Polar, M. K., Omote, H., and Figler, R. A. (2003) Transition state analysis of the coupling of drug transport to ATP hydrolysis by P-glycoprotein, *J. Biol. Chem. 278*, 52629−52640.
34. Ho, N. F. H., Raub, T. J., Burton, P. S., Bausuhn, C. L., Adson, A., Audus, K. L., and Borchardt, R. (2000) Quantitative approaches to delineate passive transport mechanisms in cell culture monolayers, in *Transport Processes in Pharmaceutical Systems* (Amidon, G. L., and Lee, P. I., Eds.) pp 219−316, Marcel Dekker, New York.
35. Shapiro, A. B., and Ling, V. (1998) Transport of LDS-751 from the cytoplasmic leaflet of the plasma membrane by the rhodamine-123-selective site of P-glycoprotein, *Eur. J. Biochem. 254*, 181−188.

36. Hyafil, F., Vergely, C., Du Vignaud, P., and Grand-Perret, T. (1993) In vitro and in vivo reversal of multidrug resistance by GF120918, an acridone carboxamide derivative, *Cancer Res. 53*, 4595−4602.
37. Polli, J. W., Wring, S. A., Humphreys, J. E., Huang, L., Morgan, J. B., Webster, L. O., and Serabjit-Singh, C. J. (2001) Rational use of in vitro P-glycoprotein assays in drug discovery, *J. Pharm. Exp. Ther. 299*, 620−628.
38. Shapiro, A. B., Corder, A. B., and Ling, V. (1997) P-glycoprotein mediated Hoechst 33342 transport out of the lipid bilayer, *Eur. J. Biochem. 250*, 115−121.
39. Tang, F., Ouyang, H., Yang, J. Z., and Borchardt, R. T. (2004) Bidirectional transport of rhodamine 123 and Hoechst 33342, fluorescence probes of the binding sites on P-glycoprotein, across MDCK−MDR1 cell monolayers, *J. Pharm. Sci. 93*, 1185−1194.
40. Rosenberg, M. F., Kamis, A. B., Callaghan, R., Higgins, C. F., and Ford, R. C. (2003) Three-dimensional structures of the mammalian multidrug resistance P-glycoprotein demonstrate major conformational changes in the transmembrane domains upon nucleotide binding, *J. Biol. Chem. 278*, 8294−8299.
41. Shitara, Y., Horie, T., and Sugiyama, Y. (2006) Transporters as determinant of drug clearance and tissue distribution, *Eur. J. Pharm. Sci. 27*, 425−446.
42. Shapiro, A. B., Fox, K., Lam, P., and Ling, V. (1999) Stimulation of P-glycoprotein-mediated drug transport by prazosin and progesterone. Evidence for a third drug-binding site, *Eur. J. Biochem. 259*, 841−850.
43. Loo, T. W., Bartlett, M. C., and Clarke, D. M. (2003) Substrate-induced conformational changes in the transmembrane segments of human P-glycoprotein. Direct evidence for the substrate-induced fit mechanism for drug binding, *J. Biol. Chem. 278*, 13603−13606.
44. Vandevuer, S., van Bambeke, F., Tulkens, P. M., and Prévost, M. (2006) Predicting the three-dimensional structure of human P-glycoprotein in absence of ATP by computational techniques embodying crosslinking data: Insight into the mechanism of ligand migration and binding sites, *Proteins: Struct., Funct., Bioinf. 63*, 466−478.
45. Omote, H., and Al-Shawi, M. K. (2006) Interaction of transported drugs with the lipid bilayer and P-glycoprotein through a solvent exchange mechanism, *Biophys. J. 90*, 4046−4059.
46. Loo, T. W., Bartlett, M. C., and Clarke, D. M. (2003) Drug binding in human P-glycoprotein causes conformational changes in both nucleotide-binding domains, *J. Biol. Chem. 278*, 1575−1578.
47. Ambudkar, S. V., Cardarelli, C. O., Pashinsky, I., and Stein, W. D. (1997) Relation between the turnover number for vinblastine transport and for vinblastine-stimulated ATP hydrolysis by human P-glycoprotein, *J. Biol. Chem. 272*, 21160−21166.
48. Hah, J. S., Ryu, J. W., Lee, W., Kim, B. S., Lachaal, M., Spangler, R. A., and Jung, C. Y. (2002) Transient changes in four GLUT4 compartments in rat adipocytes during the transition, insulin-stimulated to basal: Implications for the GLUT4 trafficking pathway, *Biochemistry 41*, 14364−14371.
49. Higgins, C. F., and Gottesman, M. M. (1992) Is the multidrug transporter a flippase? *Trends. Biochem. Sci. 17*, 18−21.
50. Borst, P., Zelcerb, N., van de Weteringa, K., and Poolman, B. (2005) On the putative co-transport of drugs by multidrug resistance proteins, *FEBS Lett. 580*, 1085−1093.
51. Hill, T. (1956) *An Introduction to Statistical Thermodynamics*, Chapter 20, Dover, New York.

BI060593B